Taylor & Francis
Taylor & Francis Group

**Vehicle System Dynamics**
International Journal of Vehicle Mechanics and Mobility

ISSN: 0042-3114 (Print) 1744-5159 (Online) Journal homepage: http://www.tandfonline.com/loi/nvsd20

# The effects of wheelset driving system suspension parameters on the re-adhesion performance of locomotives

**Yuan Yao, Shiyin Zhao, Feixiong Xiao & Jianxin Liu**

**To cite this article:** Yuan Yao, Shiyin Zhao, Feixiong Xiao & Jianxin Liu (2015): The effects of wheelset driving system suspension parameters on the re-adhesion performance of locomotives, Vehicle System Dynamics, DOI: 10.1080/00423114.2015.1108446

**To link to this article:** http://dx.doi.org/10.1080/00423114.2015.1108446

Published online: 08 Nov 2015.

*Vehicle System Dynamics*, 2015
http://dx.doi.org/10.1080/00423114.2015.1108446

# The effects of wheelset driving system suspension parameters on the re-adhesion performance of locomotives

Yuan Yao*, Shiyin Zhao, Feixiong Xiao and Jianxin Liu

*Traction Power State Key Laboratory, Southwest JiaoTong University, Chengdu, People's Republic of China*

(*Received 29 January 2015; accepted 11 October 2015*)

In this study, in order to examine the effects of a wheelset driving system suspension parameters on the re-adhesion performance of locomotives, the stick–slip vibration was analysed according to theoretical and simulation analysis. The decrease of the slip rate vibration amplitude improved the stability of the stick–slip vibration and the re-adhesion performance of locomotives. Increasing the longitudinal guide stiffness of the wheelset and the motor suspension stiffness were proposed as effective measures to improve the re-adhesion performance of locomotives. These results showed that the dynamic slip rate was inversely proportional to the series result of the square root of the longitudinal guide and motor suspension stiffness. The larger the motor suspension stiffness was, the smaller the required longitudinal guidance stiffness was at the same re-adhesion time once the wheel slip occurred, and vice versa. The simulation results proved that the re-adhesion time of the locomotive was approximately proportional to amplitude of the dynamic slip rate. When the stick–slip vibration occurred, the rotary and the longitudinal vibrations of the wheelset were coupled, which was confirmed by train's field tests.

**Keywords:** locomotive; re-adhesion performance; driving dynamics; stick–slip vibration; parameter sensitivity



## 1. Introduction

With high power railway locomotives being put into use on an increasingly large scale, it has been observed that the increases in locomotive traction and brake power have become restricted by the effective utilisation of wheel/rail adhesion. The saturation and negative slope characteristics of adhesion cause some complex dynamic problems for these locomotives.[1–11] Important theoretical and engineering applications could potentially be made if a locomotive's dynamic behaviours when undergoing saturated adhesion were more clearly understood. Also, the bogie structure parameters could be reasonably matched in order to improve the traction force and reduce the dynamic force of the mechanical structure.

The wheel/rail adhesion cannot be maintained at the peak of the W/R tangential force coefficient, and easily achieve a slip state because of the negative slope characteristics of the adhesion curves when large relative sliding occurs. Previous research has determined these

*Corresponding author. Email: yyuan8848@163.com

complex problems in the driving processes, and investigations regarding locomotives' driving dynamics began some time ago. Hirotsu et al. [1] experimentally tested the self-excited vibrations, and indicated that the increases in the stiffness, as well as the damping of locomotive structure, were helpful for restraining the vibrations. Wu [2] proposed the concept of stick–slip vibration, and analysed the vibration stability of the driving system on bogie-mounted locomotives through simulation studies. Muller and Kogel [3] analysed the wheelset rolling-slip vibrations under inconsistent adhesion on the left and right wheels. Sun [4] established a mechanical–electrical driving dynamic model, in order to study the effects on the stick–slip vibration of locomotives with different characteristics and control strategies for their electrical driving systems. Sun also proposed an integrative design principle, the 'Traction system-Bogie-Control System', for high adhesion locomotives. Some previous research data [5,6] reported the experimental investigations of the transient traction characteristics in rolling–sliding wheel/rail contacts. Polach [7,8] presented a fast wheel/rail force calculation computer code, which included the negative slope characteristics and the effects on different rail adhesion conditions. Michael [9] and Michael and Petr [10] simulated the dynamics of a torsion system of a railway driving vehicle, and analysed the main vibration frequency of a drive system during wheelset sliding, based on a measured acceleration signal. The works showed the coupling phenomena between the wheelset's longitudinal vibration and the motor pitching during the wheelset sliding. The published data of previous research of the author [11] have put forward the mechanism and dynamic characteristics of stick–slip vibration, based on the concepts of mean and dynamic slip rates. The longitudinal vibration phenomenon of the wheelset while stick–slip vibration occurs has been presented, and its formation mechanism has been clarified.

In this study, the sensitivity of the suspension parameters of the wheelset's driving system were proposed, for the performance of a high re-adhesion using a quantificational method. Also, the stick–slip vibration through the field testing of locomotives' electric braking has been presented, in order to verify the frequency coupling of the wheelset's longitudinal and driving pitch vibrations when the stick–slip vibrations occurred.

## 2. Stick–slip vibration theory [11]

### 2.1. *Slip rate*

It is well known that rigid wheel slide occurs, rather than just an elastic creep, during the driving or braking of a locomotive. In order to express the slippage in a more physical sense, the definition of the slip rate for a locomotive's driving dynamics is as follows:

$$s = \frac{v - \omega r}{v} = 1 - \frac{(\omega_0 + \dot{\theta})r}{v_0 + \dot{x}}. \tag{1}$$

Where $v$ is the instantaneous speed of the wheelset; $v_0$ is the mean speed; $\omega$ is the instantaneous angular velocity; $\omega_0$ is the mean angular velocity; $\dot{\theta}$ and $\dot{x}$ are the rotary and longitudinal vibration speed of wheelset, respectively; and $r$ is the radius of the wheel. When the macroscopic slip of the wheel occurs, the slip rate is a large but limited value, when compared to the definition of creep.[12] Under the driving conditions, $s$ is a negative value, and its absolute value is used for convenience.

As a dynamical variable, the slip rate $s$ can be written as:

$$s = s_0 + \mathrm{d}s, \tag{2}$$

where $s_0$ is the mean slip rate, and d$s$ is the dynamic slip rate. The $s_0$ depends on the traction or braking effort of the locomotive, and the adhesion condition on the rail. It was found to have a larger value during slippage. The magnitude of the d$s$ is related to the vibrant energy, and also the elastic connection of the wheelset driving system structure.

### 2.2. *Stick–slip vibration stability*

It is common knowledge that the negative slope characteristic of adhesion between the wheel and the rail is unstable, and causes the self-excited vibration of the system. The wheel/rail adhesion cannot be maintained at the peak of the W/R tangential force coefficient, and easily enters into a slip state without any control measures. The stick–slip vibration is a dynamic transition process, alternating between the stick state and slip state, and its further development depends on the system state. The stability of this process depends to a great extent on the positive and negative damping of the wheelset adhesion. In Figure 1, the symbol '$a$' represents the stick state; '$b$' represents the stick–slip state; and '$c$' represents the slip state. By ignoring the structural damping, the vibrations on stick state remain stable because the positive damping of W/R adhesion dissipates energy, and vice versa.

The negative slope characteristic of the W/R adhesion causes the system energy to increase. If $s_0$ is respectively fixed in three different constants for conditions $b$ and $c$, then the amplitude of d$s$ will increase until part of $s$ locates into a positive slope of the adhesion curves. In other words, when the system is in a stick–slip vibration state, the process of an increase and consumption of system energy are in balance, and the vibration exists in a limited cycle. Also, under condition $c$, the value of $s_0$ is greater than that of condition $b$, and a larger input energy makes it easier to change the wheelset from a slippage to stick–slip.

In regards to locomotives in service, $s_0$ cannot be a constant, and d$s$ cannot increase infinitely. As illustrated in Figure 1, when relating $a'$ with $a$, because the structural stiffness and damping of the wheelset driving system are smaller, and the vibration scope of $s$ is comparatively wider, the stick state changes into a stick–slip vibration state more easily. This causes increases in the system's vibration energy, and the slip state is more quickly reached. Likewise, when the running state of the wheelset changes from a slip into a stick, the wide vibration scope of $s$ extends the time required for the re-adhesion.

Many factors influence the re-adhesion ability of a locomotive, such as the rail surface condition, locomotive structural parameters, electric driving system, and the mechanical

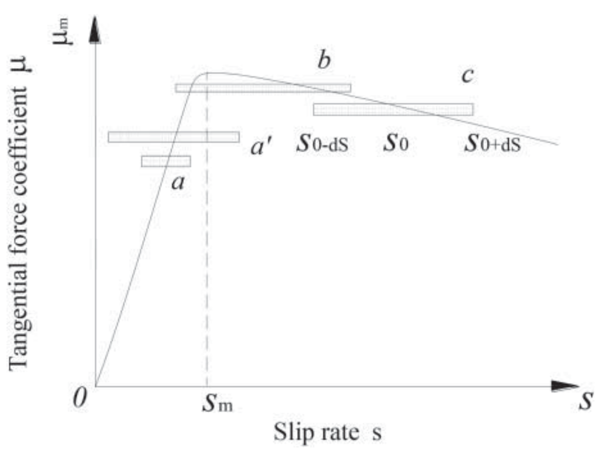


Figure 1. The different states of adhesion.

characteristics of the motor. Among these factors, the decreasing of the mean slip and the dynamic slip rates are the two most essential factors which increase the locomotive's re-adhesion ability. Therefore, for the bogie structure designs, the structural stiffness and damping of the wheelset driving system needed to be increased as soon as possible, in order to reduce the vibration scope of the slip rate.

### 2.3. *Wheelset longitudinal vibration*

By ignoring the effects of the damping from the locomotive's driving system, as well as the force from inertia, then if the slip rate is located in the *OA* section (Figure 2), and the motor torque is a constant, the positive damping will cause the system energy to decrease. Also, the angular acceleration of the wheelset will be negative. However, if the slip rate is located in the *AB* section, then the angular acceleration will be positive. When the tangential force coefficient is greater than the value of the $\mu_0$ during the periodic vibration process, which corresponds to the shaded area in Figure 2, then the wheelset's longitudinal vibration acceleration will be positive, and vice versa. During the stick–slip process of the wheelset, the minimum and maximum slip rate are respectively located on both sides of $s_0$. The minimum value will be less than the $s_c$, as shown in Figure 2. Points 1 and 2 are the corresponding tangential force coefficients of the $s_1$ and $s_2$, respectively. When the slip rate changes to a cycle of '$s_1$–$s_2$–$s_1$', the wheelset's angular velocity will be in a 'decrease-increase-decrease' cycle. However, the change process of the wheelset's longitudinal vibration velocity will be in a 'decrease-increase-decrease-increase-decrease' cycle. The wave frequency of the wheelset's longitudinal vibration acceleration will be double the frequency of the wheelset's rotary vibration acceleration. These results signify that the main frequencies of the rotary and the longitudinal vibration of the wheelset are coupled when the slick-slip vibration occurs.

The longitudinal vibration frequencies of the wheelset contain the natural frequency, along with its integral multiples of the torsional vibration of the driving system. The vibration energy reaches a maximum at twice the natural frequency. If the matching of the torsional stiffness of the driving system, and the longitudinal axle guidance stiffness of the locomotive are unreasonable, along with the wheelset longitudinal vibration frequency being an integral multiple of the rotary vibration frequency, then the stick–slip vibration will cause a strong longitudinal resonance of the wheelset. This indicates large dynamic loads, and wheel tread spalling or potential accidents affecting safety may occur.

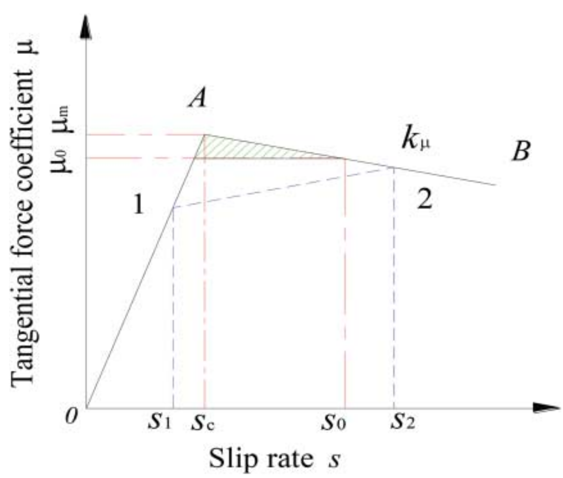


Figure 2. Graphic analysis of stick–slip vibration mechanism.

## 3. Parameter sensitivity of driving system to improve re-adhesion performance

### 3.1. *Driving dynamic model*

The locomotive driving system can be classified into two types, based on the suspension mode. These two types are the axle-mounted or nose suspension and the bogie frame suspension. The former is used for locomotives with speeds of 120 km/h. The latter is used for locomotives with a higher speed. The axle-mounted suspension of the driving system has the advantages of simple structure, large torsional stiffness, and so on. However, the bogie frame suspension has the advantages of a light unsprung mass, and excellent dynamic performances. In this study, an axle-mounted driving system used in a heavy-haul railway locomotive, with an axle power of 1600 kw, and a bogie frame suspension driving system used in a high speed locomotive with a class of 200 km/h, were adopted as the research objects. Their structural diagrams are shown in Figures 3 and 4, respectively. For the axle-mounted driving system, the pinion was supported by two bearings with a simply supported mode, in order to improve the service life of the bearing, particularly as it was used at a high axle power of 1600 kw. It required a coupling to connect the pinion and the rotor. The torsional rigidity of the coupling $K_{\mathrm{r}}$ was considered in the axle-mounted driving system's dynamic mode. One end of the driving system was mounted on the wheelset through a rolling bearing, and the other end was

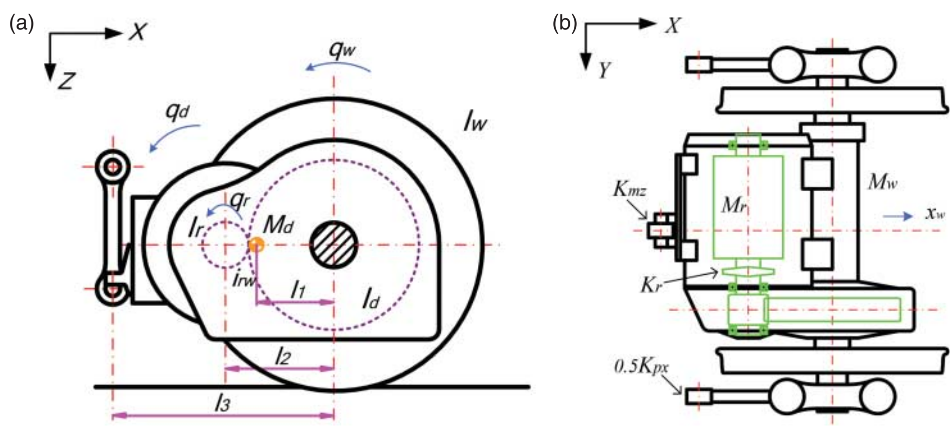


Figure 3. Axle-mounted driving system model (*Type A*).

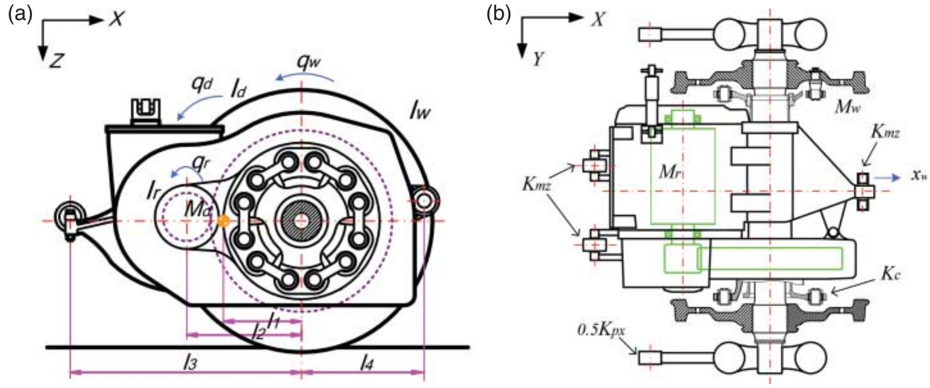


Figure 4. Bogie frame suspension driving system model (*Type B*).

Table 1. Parameters of the driving system's dynamic model.

| Symbol | Physics mean | Value $A/B$ |
|---|---|---|
| $M_{\mathrm{w}}$ | Mass of wheelset (kg) | 3731/2885 |
| $I_{\mathrm{w}}$ | Pitch inertia of wheelset (kg m$^2$) | 420/452 |
| $M_{\mathrm{d}}$ | Mass of motor stator (no including rotor of motor) (kg) | 3387/4000 |
| $I_{\mathrm{d}}$ | Pitch inertia of motor stator (no including rotor of motor) (kg m$^2$) | 370/802 |
| $M_{\mathrm{r}}$ | Mass of rotor (kg) | 100/100 |
| $I_{\mathrm{r}}$ | Pitch inertia of rotor (kg m$^2$) | 20/20 |
| $l_1$ | Longitudinal distance form mass centre of drive system to wheelset (mm) | 500/466 |
| $l_2$ | Longitudinal distance form rotor to wheelset (mm) | 800/572 |
| $l_3$ | Longitudinal distance form motor suspension rod to wheelset (mm) | 1150/1153.5 |
| $l_4$ | Longitudinal distance form motor reverse suspension rod to wheelset (mm) | – /612 |
| $K_{\mathrm{r}}$ | Rotary stiffness of rotor coupling for type $A$ (MN m rad$^{-1}$) | 13.6/ – |
| $K_{\mathrm{c}}$ | Rotary stiffness of wheelset coupling for type $B$ (MN m rad$^{-1}$) | – /7 |
| $K_{\mathrm{m}z}$ | Motor vertical suspension stiffness (kN mm$^{-1}$) | 10/64 |
| $K_{\mathrm{p}x}$ | Longitudinal axle guidance stiffness (kN mm$^{-1}$) | 44.14/57.34 |
| $i$ | Transmission ratio of gear transmission | – 6.2941/ – 3.91 |

suspended under the bogie frame through a rod. A six-bar double hollow shaft coupling was used to transfer the motor torque, and to adapt the relative motion between the driving system and wheelset in the bogie frame suspension driving system. The equivalent torsional stiffness of the six-bar double hollow shaft coupling was $K_{\mathrm{c}}$, and the driving system was hung under the bogie frame by one rubber joint and two pendulums.

The two types of driving systems were equivalent to a uniform dynamic model, which consisted of a wheelset and a motor stator, as well as a motor rotor. The wheelset had the freedom to move longitudinally, as well as rotate along the $Y$ axle. The motor stator and rotor had the freedom to rotate along the wheelset and the rotator centre, respectively. The detailed parameters of the driving system's dynamic model are as shown in Table 1. This dynamic mode was established to analyse the stick–slip vibration caused by the change of the wheel/rail adhesion force or driving torque, and the main vibration was reflected in the wheelset's longitudinal and rotation directions. When the W/R was in a state of adhesion, the vibration of the wheelset was vertical, and the rotational direction could be seen as a decoupling. This driving system model could be simplified into a torsional vibration model of the drive system and a longitudinal vibration model of the wheelset.

### 3.2. *Simplified dynamic model*

#### 3.2.1. *Equivalence principle of system parameters*

In regards to a gear transmission system, the system parameters of the input or output axis can be equivalent to the same axis, according to the principle of equivalence to analyse torsional vibration. According to kinetic energy conservation, the equivalent moment of inertia is as follows:

$$I_{\mathrm{e}} = I \cdot i^2. \tag{3}$$

According to the potential energy conservation, the equivalent torsional stiffness is as follows:

$$k_{\theta\mathrm{e}} = k_\theta \cdot i^2. \tag{4}$$

The equivalent of the torque is as follows:

$$T_{\mathrm{e}} = T \cdot i^2. \tag{5}$$

### 3.2.2. *Simplified torsional model of driving system*

The motor stator applies the electromagnetic torque to the rotor, and drives the wheelset along the track through gear transmissions as a locomotive pulls a train. Due to the pitch degree of freedom of the motor stator around the wheelset, the pitch angle of the motor stator appears under the action of the driving torque. The pitch stiffness of the motor is dependent on the vertical suspension stiffness and the longitudinal distance from the suspension rod to the wheelset, or from the rubber joints to the pendulums. According to the transmission path of the torque, the motor rotor, stator, and wheelset are connected in a series. The moment of the inertia of the motor rotor and the stator, as well as the torsional stiffness, are equivalent to the axle of the wheelset. The equivalent torsional model is as shown in Figure 5.

When the rotor rotational speed is equal to 0, the transmission ratio from the pitch movement of the motor stator to the wheelset rotation is as follows:

$$i_{\mathrm{dw}} = \frac{i}{i-1}. \tag{6}$$

The equivalent moment of the inertia $I_{\mathrm{re}}$ and $I_{\mathrm{de}}$ and the equivalent torsional stiffness $k_{\mathrm{re}}$ and $k_{\mathrm{de}}$ of the rotor and motor stator to the wheelset can be calculated according to Equations (3) and (4). Due the fact that the equivalent torsional stiffness is proportional to the square of transmission ratio, the equivalent torsional stiffness of rotor $k_{\mathrm{re}}$ can be seen as rigid.

When the wheel/rail is in an adhesion state, that is to say, in a positive slope of the adhesion characteristic curve, then the transmission ratio from the longitudinal movement to the rotation movement of the wheelset is $R$. The equivalent moment of the inertia $I_{\mathrm{we}}$ of the wheelset is as follows:

$$I_{\mathrm{we}} = R^2 M_{\mathrm{w}x} + I_{\mathrm{w}}, \tag{7}$$

Where $R$ is the rolling radius of wheelset; $M_{\mathrm{w}x}$ represents the locomotive longitudinal unsprung mass; and $M_{\mathrm{w}x}$ equals $M_{\mathrm{w}}$, plus $M_{\mathrm{d}}$, as well as $M_{\mathrm{r}}$.

When the wheel/rail is in a pure sliding state, that is to say, in a negative slope of the adhesion characteristic curve, then the equivalent moment of the inertia $I_{\mathrm{we}}$ equals $I_{\mathrm{w}}$.

The $k_{\mathrm{c}}$ is the connected stiffness from the motor stator to the wheelset, as illustrated in Figure 5. For the axle-mounted suspension drive system, the $k_{\mathrm{c}}$ can almost be rigid. While in the bogie frame suspension drive system, the $k_{\mathrm{c}}$ cannot be ignored, and it is dependent on the torsional stiffness of connect component, such as the six-bar double hollow shaft, or other cardan couplings.

The equivalent torsional stiffness of motor rotor to wheelset equals the torsional stiffness of rotor multiplied by the square of the gear transmission ratio, and this result is of great value. Therefore, the effect of the torsional stiffness of the rotor to pinion on the stick–slip vibration of the wheelset can be ignored. The drive system torsional vibration model can be further simplified, as shown in Figure 6(a), where the $k_{\mathrm{t}}$ is a composite stiffness of the $k_{\mathrm{de}}$ and $k_{\mathrm{c}}$. In regards to the analysis of the free response of the rotary vibration of the wheelset under

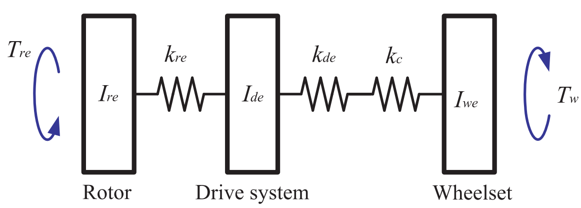


Figure 5. Torsional vibration system model.

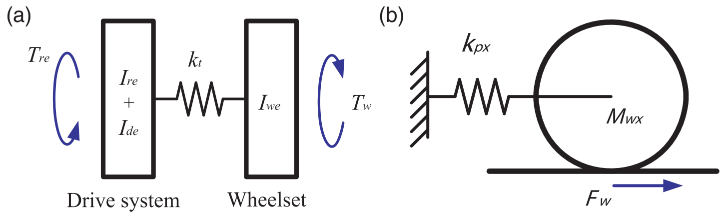


Figure 6. Simplified torsional vibration and wheelset longitudinal vibration system model.

an external impulse, the model can be further simplified as a single degree of freedom, which only has a rotary degree of freedom of the wheelset. The equivalent principle is to ensure that the vibration frequency of the original and the equivalent models are consistent, by changing the torsional stiffness $k_{\mathrm{te}}$ according to the following formula (Equation (8)):

$$k_{\mathrm{te}} = k_{\mathrm{t}}\left(1 + \frac{I_{\mathrm{we}}}{I_{\mathrm{re}} + I_{\mathrm{de}}}\right). \tag{8}$$

The natural vibration frequency of the torsional vibration of the driving system is as follows:

$$f_{\mathrm{w}\theta} = \frac{1}{2\pi}\sqrt{\frac{k_{\mathrm{te}}}{I_{\mathrm{we}}}}. \tag{9}$$

### 3.2.3. *Simplified longitudinal vibration model of wheelset*

The transfer path of the locomotive longitudinal force was from the wheelset to the bogie frame, and then to the car body. Since the mass of car body was larger, the longitudinal vibration frequency of the unsprung mass depended on the axle guidance stiffness, mainly when the longitudinal stiffness of the drawbar was a larger value. In this study it was assumed that the drawbar longitudinal stiffness was large enough for a theoretical analysis.

The simplified wheelset longitudinal vibration model is shown in Figure 6(b). Due to the transmission ratio from the rotary to the longitudinal movement of the wheelset equalling $1/R$, the influence of the rotational inertia of the wheelset on longitudinal vibration can be ignored.

The natural vibration frequency of the longitudinal vibration of the wheelset is as follows:

$$f_{\mathrm{w}x} = \frac{1}{2\pi}\sqrt{\frac{k_{\mathrm{p}x}}{M_{\mathrm{w}x}}}. \tag{10}$$

## 3.3. *Suspension parameters matching principle*

The dynamic amplitude of the longitudinal vibration speed of the wheelset was less than the average running speed, when the locomotive operated at high speeds. Assuming the denominator in Equation (1) is a constant, the slip rate can be written as follows (Equation (11)):

$$s \approx s_0 + \frac{\dot{x}}{v_0} - \frac{R \cdot \dot{\theta}}{v_0}. \tag{11}$$

When the amplitude of the dynamic slip rate was smaller, improvements in the re-adhesion ability of the locomotive according to the stick–slip vibration theory were observed.

Therefore, it was very important to reduce the dynamic amplitude of the longitudinal and rotational vibration of the wheelset. Based on the simplified dynamic model of the wheelset driving system, the wheelset free vibration at the direction of the longitudinal, and the rotary under a rectangular pulsed excitation was analysed. The given longitudinal wheel/rail force acting on the simplified model is as follows:

$$F_{\mathrm{w}}(\tau) = \begin{cases} F_0 & 0 \le \tau \le t_1, \\ 0 & \tau > t_1, \end{cases} \tag{12}$$

where $F_0 = L_{\mathrm{w}} g \mu \cdot L_{\mathrm{w}}$ is the axle-load of the locomotive (25 $t$ in this study); $g$ is the acceleration of gravity; and $\mu$ is the wheel/rail friction coefficient.

According to the Duhamel integral,[13] the response speed of the undamped free vibration of a single DOF vibration system is:

$$\dot{y} = \frac{2F_0}{\sqrt{m \cdot k}} \sin\frac{\omega_n t_1}{2} \cos\left(\omega_n t - \frac{\omega_n t_1}{2}\right), \tag{13}$$

where $m$ and $k$ are the mass and stiffness of the single DOF system; and $\omega_n$ is the natural frequency.

It can be seen from Equation (13) that the response speed amplitude of the free vibration is related to $t_1$ and $\omega_n$. The results of $t_1$ multiplied by $\omega_n$ is assumed to be equal to $\pi$. Therefore, the vibration speed amplitude decreased with the increasing of the mass and stiffness of the vibration system.

The free vibration speed amplitudes of the wheelset at the longitudinal direction and rotary of the simplified dynamic model under the longitudinal force are as shown in the following expression:

$$\dot{\theta}_{\mathrm{w}} = \frac{2F_0 R}{\sqrt{k_{\mathrm{te}} I_{\mathrm{w}}}}, \tag{14}$$

$$\dot{x}_{\mathrm{w}} = \frac{2F_0}{\sqrt{k_{\mathrm{p}x} M_{\mathrm{w}x}}}. \tag{15}$$

The dynamic slip rate (d$s$) of wheelset is:

$$\mathrm{d}s = \frac{2F_0}{v_0}\left(\frac{1}{\sqrt{k_{\mathrm{p}x} M_{\mathrm{w}x}}} + \frac{R^2}{\sqrt{k_{\mathrm{te}} I_{\mathrm{w}}}}\right). \tag{16}$$

The parameters of *Tape A* in Table 1 are substituted into Equation (16), and the equation can be written as:

$$\mathrm{d}s = \frac{23.5F_0}{v_0}\left(\frac{1}{\sqrt{k_{\mathrm{p}x}}} + \frac{0.95}{\sqrt{k_{\mathrm{m}z}}}\right) \times 10^{-3}. \tag{17}$$

It was apparent that the dynamic slip ratio was inversely proportional to the series result of the square root of $k_{\mathrm{p}x}$ and $k_{\mathrm{m}z}$. Only increasing one of the suspension stiffness had no remarkable effect for decreasing the d$s$. In addition, the weight coefficient of the square root of the $k_{\mathrm{m}z}$ was 0.95 times that of the $k_{\mathrm{p}x}$, which means that their influences were at the same level.

Figure 7 shows the contour of the dynamic slip rate of the axle-mounted driving system at the different motor vertical suspension stiffness and longitudinal axle guidance stiffness of the wheelset. The horizontal and vertical logarithmic coordinates were the longitudinal axle

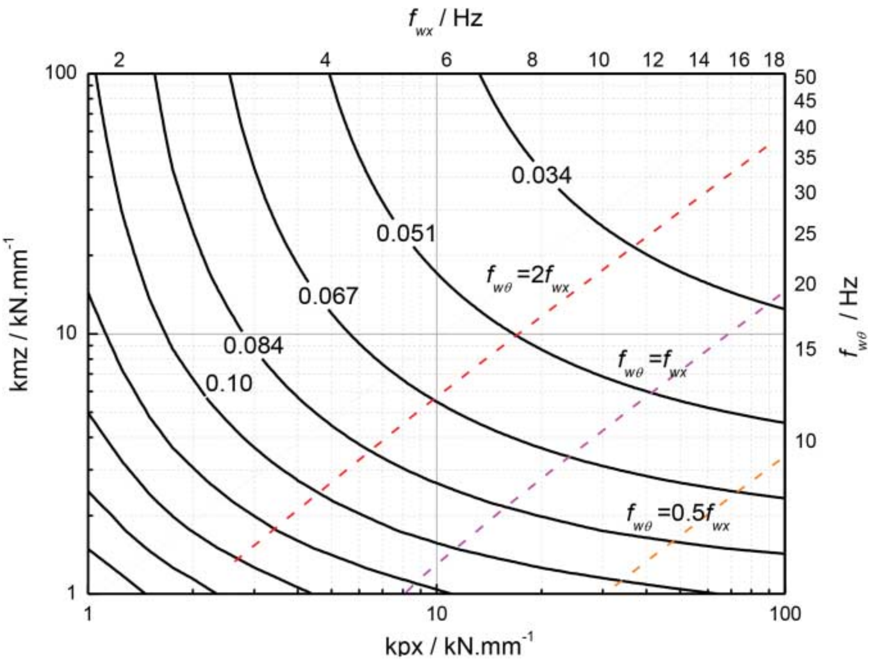


Figure 7. Contour of the d$s$ at the different of $k_{px}$ and $k_{mz}$ of the axle-mounted driving system.

guidance stiffness of the wheelset, and the motor vertical suspension stiffness, as well as the corresponding natural frequency, respectively. The curve represents the same amplitude of the dynamic sliding rate. The oblique dashed line represents the stiffness values with which the corresponding nature frequency was an integer multiple to another nature frequency, which

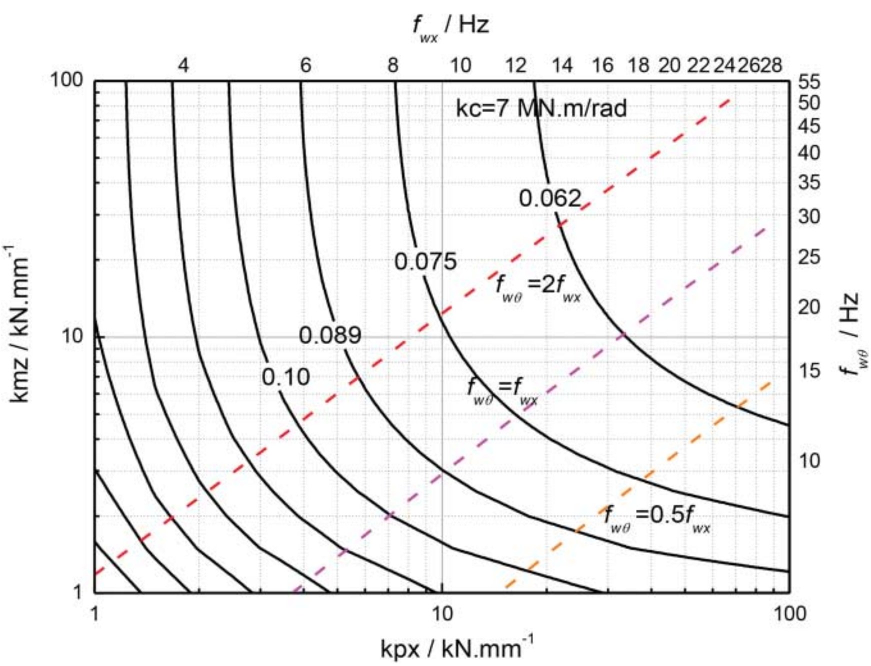


Figure 8. Contour of the d$s$ at the different $k_{px}$ and $k_{mz}$ of the bogie frame suspension driving system.

means that the resonance occurred when in a saturated adhesion. The larger the motor suspension stiffness was, the smaller the required longitudinal guidance stiffness was at the same dynamic slip rate, and vice versa. For example, the $k_{px}$ and $k_{mz}$ of wheelset driving system adopt the following two sets of suspension parameters, such as (15 kN/mm, 100 kN/mm) and (40 kN/mm, 20 kN/mm), the locomotive has a close re-adhesion performance under the same conditions.

Figure 8 shows the contour of the dynamic slip rate of the bogie frame suspension driving system at different motor vertical suspension stiffnesses, and the longitudinal axle guidance stiffness of the wheelset. It was assumed that the vertical stiffness of the three rubber joints connected to bogie frame were the same. The curves were similar to an ellipse. The difference compared to *Type A* was that the coefficient of $k_{mz}$ item was 2.6 in this driving system, which means that there was more of a distinct effect of the $k_{mx}$ on the d$s$ of *Type B* than $k_{mz}$ in the calculated parameter domain. Due to the series torsional stiffness of the six-bar double hollow shaft coupling being taken into account, the d$s$ was found to have a larger value than that in the *Type A*.



## 4. Simulation analysis of locomotive re-adhesion performance

### 4.1. *System dynamics model*

A dynamics model of a train system was established with the software program SIMPACK. This model was composed of a locomotive and ten vehicles, as shown in the research data.[11] The train hauling load was considered, and the unit vehicle was simulated by a mass block which had a single degree of freedom along the track direction, where the mass blocks were connected by a coupler force. The axle loads of the locomotive and the vehicle were 23 and 21 t, respectively. The locomotive was equipped with a Co′Co′ axle arrangement, and the uniaxial power was 1600 kW. The locomotive driving system adopted an integral structure, where the gear box was installed on the wheelset, and could be rotated around it. The motor was suspended under the frame by a rod. This driving system model (Type *A*) included a motor, gearbox, rotor, hang rod, pinion and large gear, and their detailed parameters are as shown in Table 1. The high-power locomotive driving system used a flexible coupling between the rotor and pinion, and the torsional stiffness of the flexible coupling was 1.36e7 N m/rad.

The train's resistance was composed of the basic resistance, and the additional resistance of the ramp way. The train ran uniformly when the locomotive traction force and resistance were balanced. In this study, the dynamic model adopted a JM3 worn-type wheel tread and a standard 60 kg/m rail shape. The dynamic model was able to simulate the actual dynamic processes during the locomotive's traction operation. This model also covered more uncertain factors in the locomotive's adhesion control.

### 4.2. *Characteristics of W/R adhesion*

The tangential force coefficient decreased with the increase in the W/R slip velocity.[14] These results corresponded to the negative slope characteristic of the adhesion curves. According to previous investigations,[6,7,11,14] the adhesion curves were different with different rail surface conditions. These differences include: the maximal tangential force coefficient; the slip rate corresponding to this maximal tangential force coefficient; the linear slope near the origin; and the negative slope at the slippage. These can be defined as the four factors of adhesion.[15,16] The W/R friction coefficient $f$, as a function of the contact patch sliding velocity,[17] can be written as:

$$f = \frac{f_s}{1 + F\upsilon_c}. \tag{18}$$

In Equation (18), $f_s$ is the static friction coefficient; $F$ is the dynamic friction effect coefficient, which equals 0.23 in this study; and $\upsilon_c$ is the sliding velocity of the contact patch.

By modifying the W/R tangential force calculation program of Shen et al.,[18] in accordance with Equation (18), the wheel/rail tangential force coefficient curves, including the negative slope characteristic, can be obtained. With the increase of the locomotive velocity, the negative slope characteristic became obvious. In addition, by changing the Kalker weight coefficient $K$, and the dynamic friction influence coefficient $F$, the four factors of the adhesion curves were simulated. The reduction of the coefficient $K$ tended to reduce the slope of the linear segment, in order to simulate wet track surface conditions. Also, increasing $F$ was found to increase the negative slope of the adhesion curve. Thereby, the different shapes of the tangential force coefficient curves were obtained.[11,15,16]

### 4.3. *Electric drive system and control*

The high power locomotives have adopted an ‘AC–DC–AC’ traction driving system. The motor’s electric drive model and constant speed control were used in this study, as shown in [11]. It should be noted that the model considers only the mechanical characteristics of the driving motor, and does not use the adhesion control unit.

### 4.4. *Effects of suspension parameters on re-adhesion performances*

The operating condition of train running on a straight line with an initial velocity of 80 km/h was simulated with the above mentioned electrical transmission model. The W/R contact static friction coefficient $f_s$ is shown in Figure 14 in reference [11]. The horizontal axis is time and the vertical axis is the friction coefficient of rail. With the decrease of $f_s$ slippage occurred, and then the adhesion recovered after 8 s. When the $f_s$ decreases and recovers, the wheelset changes into the stick–slip vibration state. The track irregularity was not taken into account in the simulation model, in order to make the process of the stick–slip vibration more obvious.

Figures 9 and 10 show the influence of the different wheelset driving system suspension parameters on the stick–slip vibration. It was revealed that the longitudinal axle guidance stiffness and the motor suspension stiffness had significant effects on the stick–slip vibration. With the increase of these suspension parameters, the re-adhesion ability of the locomotive increased. The wheelset went into the slip state when the $f_s$ decreased. However, when the $K_{px}$ became larger, the wheelset entered directly into a full slip state, and then the W/R adhesion negative damping raised the system’s vibration energy, enlarged the vibration scope of the longitudinal slip rate, and the wheelset entered into a stick–slip state before the $f_s$ increased. Then, the wheelset quickly returned to the stick state when the $f_s$ began to increase. With smaller $K_{px}$, the vibration scope of the slip rate was larger, and stick–slip vibration occurred. The wheelset gradually transformed into a full slip state when the $f_s$ began to decrease. When the $f_s$ increased, the wide scope of the slip rate prolonged the recovery adhesion time. The simulation results were consistent with the conclusions of the stick–slip vibration stability shown in Section 2.2.

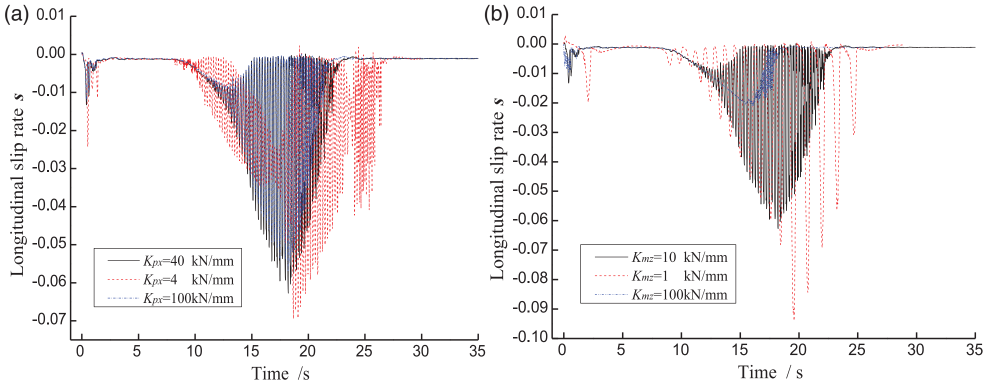


Figure 9. (a) Effect of the longitudinal guide stiffness of the wheelset on stick–slip vibration and (b) effect of motor suspension stiffness on stick–slip vibration.

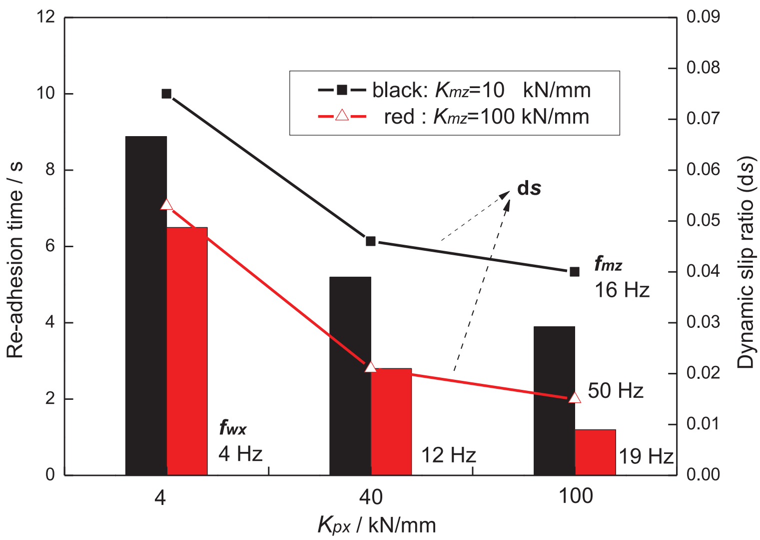


Figure 10. Relationship of re-adhesion time and dynamic slip rate.

Figure 9(a) shows the simulation of the longitudinal slip rate, with respect to the different motor suspension stiffness. When the motor suspension stiffness increased, the recovery adhesion time decreased. Figure 9(b) also indicates that the smaller the motor suspension stiffness was, the larger the wheelset longitudinal slip rate was, the longer the recovery adhesion time was, and the lower the locomotive's re-adhesion ability was. In addition, the frequency of the wheelset's longitudinal slip rates depended mainly on the motor suspension stiffness, which confirms the conclusion that the wheelset's longitudinal vibration frequency depends on the driving system's torsional stiffness, as concluded in Section 2.3.

Figure 10 shows the simulated re-adhesion time of the locomotive, and the dynamic slip rate according to Equation (16) at the different longitudinal guides and motor suspension stiffnesses. The calculated dynamic slip rates by Equation (16) were at the same level as the simulation results of Figure 9(a) and 9(b). The calculated dynamic slip rate decreased with the increasing of the suspension stiffness of the wheelset's driving system, and the corresponding simulated re-adhesion time reduced, which is consistent with the theoretical analysis.

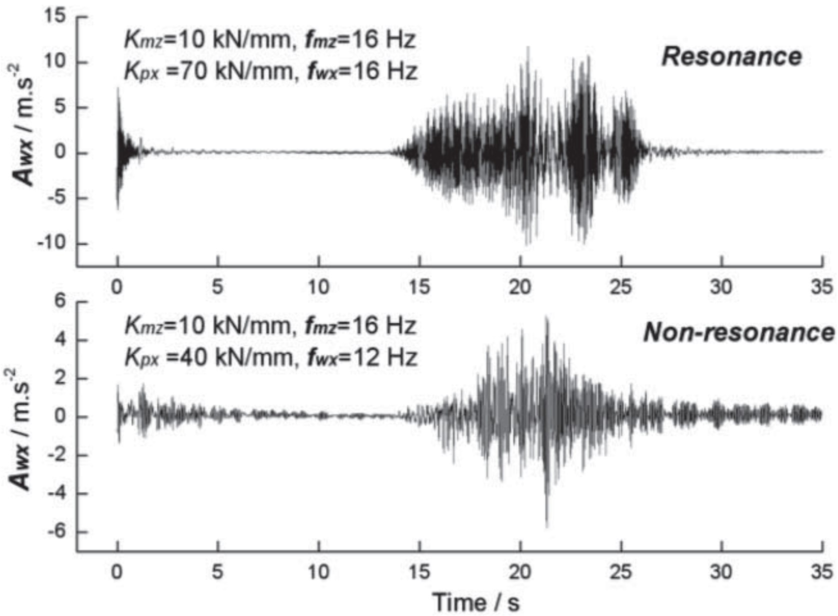


Figure 11. Simulated longitudinal vibration acceleration of the wheelset.

Although the re-adhesion time was not in strict proportion with the dynamic slip rate, these results are significant to engineering guidance.

Figure 11 shows the simulated longitudinal vibration acceleration of the wheelset when the stick–slip vibration occurred, with the condition that the natural vibration frequencies of the wheelset and motor were respectively consistent and not consistent. It was clear that once the stick–slip vibration occurred, a structural resonance occurred if the natural vibration frequencies of wheelset and motor were consistent, which caused a larger vibration amplitude of the wheelset's driving system, and extended the re-adhesion time of the locomotive.

## 5. Field tests

The locomotive tested pulled a 10,000 ton coal train running, which equipped with drive systems of *Type A*, at a long down ramp approximately 30 km in length, with a gradient of 13%. The train ran at a speed of approximately 75 km/h. The braking force was only supplied by the electric brake of the locomotive, but the train's air brake was used on the down ramp. Most of the time, the braking current could reach 90% of maximum current and braking force of single wheelset reaches 75 kN. During the braking, the locomotive experienced a larger longitudinal coupler compressive force, and it had to stand continuously in order to ensure that the wheelset did not slip. The process of locomotive electric braking is similar to the driving process, just as the torque direction of motor is the opposite. The slip and re-adhesion of the wheelset undergoing motor braking torque are consistent with the stick–slip vibration which is caused by the driving torque.

The longitudinal vibration acceleration of wheelset driving system was tested, and the acceleration sensor was attached to the driving system as show in Figure 12. The sensor's maximum range was 10 g and the sampling frequency was 1 K. The locomotive ran under

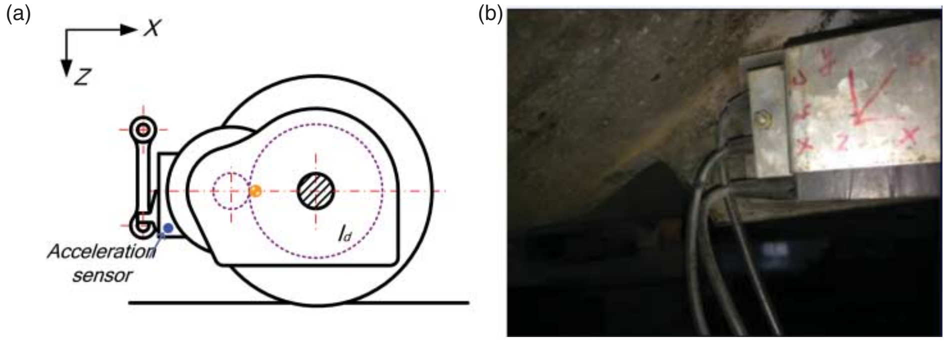


Figure 12. The position of acceleration sensor in field tests.

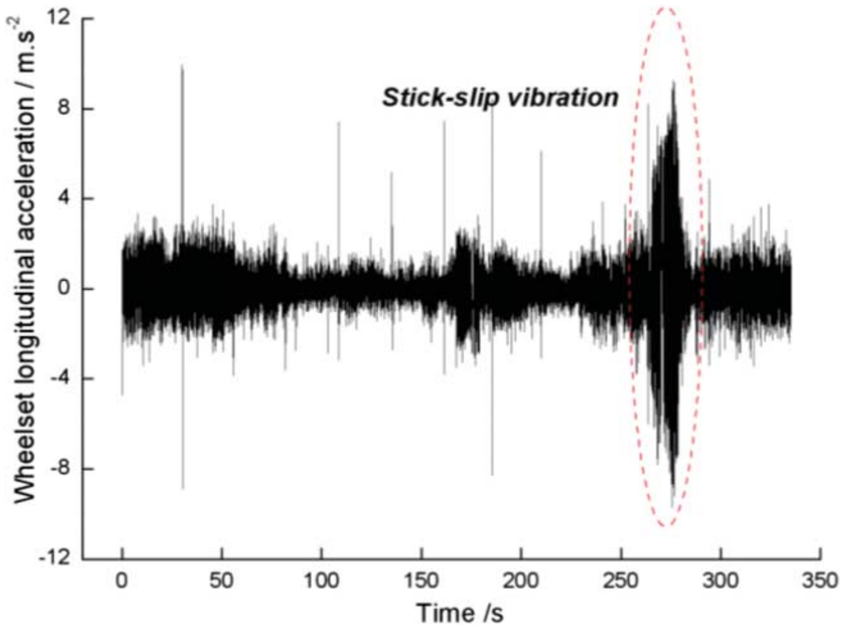


Figure 13. Test results of the wheelset's longitudinal vibration acceleration.



normal operating conditions, and a segment of the wheelset driving system's longitudinal vibration acceleration is shown in Figure 13. The acceleration increased in an obvious way at the time of 260 to 280 s, at which timeframe the stick–slip vibration occurred. The longitudinal acceleration amplitude spectrum of the wheelset driving system at the stick–slip vibration occurred and did not occur, as shown in Figure 14. It showed that the main vibration frequency of the wheelset was 12 Hz when stick–slip vibration did not occur. Meanwhile, the main vibration frequency of the wheelset was 12 and 16 Hz when stick–slip vibration did occur, and the 16 Hz was the natural frequency of motor pitching. In regards to the two times when motor pitching frequency did not occur, this may have been caused by the bandwidth limiting of the acceleration sensor, or by the rapid decreasing of the high-frequency vibration due to the damping. The field tests confirmed the theoretical analysis conclusions, as well as the simulation results.

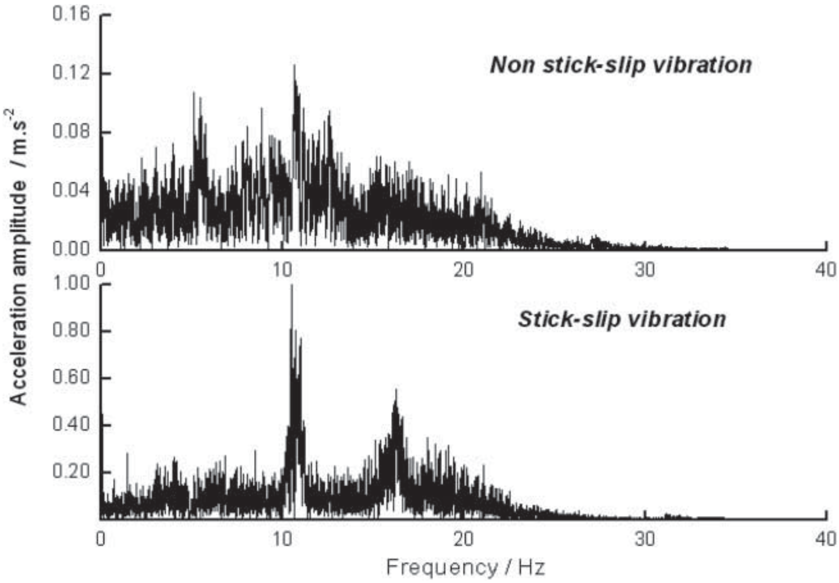


Figure 14. Amplitude spectrum of the wheelset's longitudinal acceleration.

## 6. Conclusions

(1) The stick–slip vibration was analysed according to the mean and the dynamic slip rate, and the decreasing of the dynamic slip rate was found to improve the stability of the stick–slip vibration. The increasing of longitudinal guide stiffness of the wheelset and motor suspension stiffness were effective measures for decreasing the dynamic slip rate, as this resulted in the improvement of the re-adhesion performance of the locomotive.
(2) The dynamic slip rate was inversely proportional to the series result of the square root of the longitudinal guide stiffness and the motor suspension stiffness. The larger the motor suspension stiffness was, the smaller the required longitudinal guidance stiffness required at the same dynamic slip rate was, and vice versa. For the axle-mounted driving system, the effects of the two suspension parameters on the dynamic slip rate were at the same level. The simulation results proved that the re-adhesion time of the locomotive was approximately proportional to the dynamic slip rate amplitude.
(3) When the stick–slip vibration occurred, the rotary and the longitudinal vibrations of the wheelset were coupled with the longitudinal tangential force. A structure resonance of the wheelset's driving system will occur if the natural vibration frequencies of the wheelset and motor are consistent, which causes a larger vibration amplitude, and extends the re-adhesion time of the locomotive. The train's field tests confirmed the phenomenon of a frequency coupling under saturated adhesion.

## Disclosure statement

No potential conflict of interest was reported by the authors.


## Funding

The authors wish to acknowledge the support of the National Natural Science Foundation of China (No. 51205324, 51375403), the Fundamental Research Funds for the Central Universities (No. 2682014CX040) and the Independent Research and Development Projects of a Key Laboratory grant (No. 2015TPL_T10).

## References


[1] Hirotsu T, Kasai S, Takai H. Self-excited vibration during slippage of parallel cardan drives for electric railcars. JSME Int J. 1987;30:1304–1310.

[2] Wu YF. Stability analysis of the vibration of the frame-mounted motor driving system. J China Rail-way Soc. 1992;14:1–7.

[3] Muller S, Kogel R. Numerical simulation of roll-slip oscillations in locomotive drives. Z Angew Math Mech. 2001;81:61–64.

[4] Sun X. The locomotive system design of high adhesion performance. J Southwest Jiaotong Univ. 1994;29:235–247.

[5] Koansok B, Keiji K, Tsunamitsu N. An experimental investigation of transient traction characteristics in rolling–sliding wheel/rail contacts under dry–wet conditions. Wear. 2007;263:169–179.

[6] Zhang WH, Chen JZ, Wu XJ. Wheel/rail adhesion and analysis by using full scale roller rig. Wear. 2002;253:82–88.

[7] Polach O. Influence of locomotive tractive effort on the forces between wheel and rail. Veh Syst Dyn. 2001;35:7–22.

[8] Polach O. A fast wheel-rail force calculation computer code. Veh Syst Dyn. 1999;33:728–739.

[9] Michael L. The modern wheelset drive system and possibilities of modeling the torsion dynamics. Transport. 2008;23:172–181.

[10] Michael L, Petr V. Identification of transient phenomena occurring at the initiation and termination of wheelset sliding. Transport. 2012;27:86–91.

[11] Yao Y, Zhang HJ, Luo SH. An analysis of resonance effects in locomotive drive systems experiencing wheelrail saturation adhesion. Rail Rapid Transit. 2014;228(1):4–15.

[12] Wang FT. Vehicle system dynamics. Shanghai: Shanghai Railway University Press; 2004.

[13] Wen BC. Theory of mechanical vibration and its applications. Beijing: Higher Education Press; 2009.

[14] Ertz M, Knothe K. Thermal stresses and shakedown in wheel/rail contact. Arch Appl Mech. 2003;72:1521–1533.

[15] Yao Y, Zhang HJ, Luo Y. Torsional-longitudinal coupling vibration analysis of drive system on locomotive. J Traffic Transp Eng. 2009;9:13–17.

[16] Yao Y, Zhang HJ, Chen K. Self-excited torsional vibrations of drive system on locomotive under slippage. J Southwest Jiaotong Univ. 2008;43:762–766.

[17] Jin XS, Zhang LM. Numerical analysis of the driving torque applied to a single wheelset of locomotive with high speed. Chinese J Mech Eng. 1999;35:56–60.

[18] Shen ZY, Hedrick JK, Elkins JA. A comparison of alternative creep-force models for rail vehicle dynamic analysis. Proc, 8th IAVSD Symp., Cambridge, Ma.; 1984. p. 591–605.